Received: 20 May 2024 | Revised: 26 July 2024 | Accepted: 2 September 2024

DOI: 10.1002/ese3.1919

ORIGINAL ARTICLE

Synergetic effect of iron and tungsten on molybdenum-doped HZSM-5 zeolite in catalytic methane dehydroaromatization

Ronald. W. Musamali[1] | **Yusuf. M. Isa**[2]

[1]The Technical University of Kenya, Nairobi, Kenya

[2]School of Chemical and Metallurgical Engineering, University of the Witwatersrand, Johannesburg, South Africa

Correspondence
Yusuf. M. Isa, School of Chemical and Metallurgical Engineering, University of the Witwatersrand, Johannesburg, 2001, South Africa.
Email: yusuf.isa@wits.ac.za

Abstract

Methane dehydroaromatization is a viable route for production of carbon and valuable petrochemicals. Unlike Fischer–Tropsch and methanol synthesis processes which have been scaled up to commercial level, development of methane dehydroaromatization to commercial level has been hampered by various challenges. In this work, a 5.4 wt. % trimetallic (Fe-W-Mo/HZSM-5) catalyst has been synthesized, characterized, and applied in catalytic methane dehydroaromatization reaction. A gas chromatograph was used to analyze both liquid and gaseous products from the reactor. Based on 0.0013 moles of reacted methane after 240 min time on stream at 750°C, GHSV 960 $mlg^{-1}cath^{-1}$, and atmospheric pressure, a 5.4% Mo/HZSM-5 catalyst recorded 7.9% methane conversion, 10.6% C_2 hydrocarbon selectivity, 51.8% benzene selectivity, 9.8% toluene selectivity and 27.8% coke selectivity. Doping Mo/HZSM-5 with Fe reduced methane conversion by 4.0%, increased C_2 hydrocarbon selectivity by 1.7%, reduced benzene selectivity by 6.2% and increased toluene and coke selectivity by 1.8% and 2.8% respectively. Doping Mo/HZSM-5 with W increased methane conversion by 7.3%, reduced C_2 hydrocarbon selectivity by 2.1%, reduced benzene selectivity by 7.6% and increased toluene and coke selectivity by 0.3% and 9.4% respectively. When iron and tungsten were loaded onto Mo/HZSM-5, catalytic activity of the tri-metallic catalyst in methane conversion reduced by 2.0%, C_2 hydrocarbon selectivity increased by 2.7%, benzene selectivity reduced by 3.1%, toluene selectivity reduced by 3.7%, and coke selectivity increased by 4.1%. Therefore, this present work demonstrates that metal synergy in a tri-metallic catalyst plays a role in methane conversion and selectivity towards useful hydrocarbons.

KEYWORDS

catalyst synergy, hydrocarbon selectivity, metal doping, methane conversion, trimetallic catalyst

1 | INTRODUCTION

Generation of energy from fossil fuels is associated with emission of greenhouse gases which are harmful to the environment.[1]

Natural gas is the cleanest fossil fuel and is a safe source of energy when transported and used carefully.[2] Methane is the major component of natural gas although, it may also contain traces of C_2 hydrocarbons, N_2, CO_2, He, H_2S, and noble gases. Methane is the most stable symmetric organic molecule consisting of C-H covalence bond, with bond energy of 435 kJ/mol. Effective activation and direct methane conversion to fuels and petrochemicals is attracting interest from many researchers.[3] Successful conversion will be applicable to biomethane which is a positive shift towards sustainable bioeconomies.

Methane conversion into value-added products is an area of interest to present day researchers. This follows the successful scale-up of Fischer–Tropsch[4] and methanol synthesis[5] to commercial levels. However, an attempt to fully exploit methane dehydroaromatization has been faced with various challenges such as, high equipment cost, catalyst deactivation, process thermodynamics, low conversion, and limited product selectivity.[6] Most research in this area has been built around Mo/HZSM-5 catalyst which was first reported in 1993 by.[7] A major drawback to this invention is the formation of reactive coke which is responsible for catalyst deactivation. An attempt to address this problem by various research groups include among others the addition of small amounts of oxygen,[8] hydrogen,[9] and water[10] in methane feed. Despite intensive research in this area, catalyst selectivity towards C_2 hydrocarbons has remained low and selectivity towards higher carbon hydrocarbons >80% has not been reported.[11]

Remarkable catalyst activity using single metal catalyst systems has been achieved at reaction temperature >800°C yielding carbon and petrochemicals such as; hydrogen, ethane, ethylene, propylene, benzene, heptane, octane, and decane.[12]

In the last three decades, methane dehydroaromatization reaction has been studied by,[13,14] and[15] over Mo/HZSM-5 catalyst. In their work, it was claimed that hydro condensation of methane into benzene was as a result of interaction of carburized molybdenum species and the acid sites inside the HZSM-5 channels. Further,[16] and[17] revealed that hydro condensation of methane into aromatics and higher carbon hydrocarbons could be achieved on bimetallic Co-Mo/HZSM-5. To address coking problem in methane dehydroaromatization reaction, intense research work has focused on suppressing coke formation and enhance product selectivity. Much work in methane dehydroaromatization has focused on improvement of catalyst structural properties,[18] promotion with metals,[19] and periodic (CH_4/H_2) switching[20] to increase the number of acid sites on zeolite support.

Modification of Mo/HZSM-5 with noble metals have been greatly studied and found to have a great influence on methane conversion, product distribution, and catalyst deactivation by coking.[19] Iron has been touted as one of the best catalysts in Fischer Tropsch reaction because it promotes chain growth of light hydrocarbons via C-C coupling mechanism[21] and improves catalyst stability.[22] From their findings, Fe initially suppresses benzene formation while inducing the formation of carbon nanotubes (CNT). This is helpful in preventing HZSM-5 from agglomeration to accelerate reactant and product diffusion process thereby increasing benzene yield. Promotion of Mo/HZSM-5 with Zn[23] and W[24] enhanced catalyst stability and selectivity towards benzene yields. However,[22] did not observe any remarkable catalyst activity of Zn-Mo/HZSM-5 catalyst in methane dehydroaromatization reaction. Therefore, studies on metal synergy in double promotion of Mo/HZSM-5 has not been exhaustively reported in methane dehydroaromatization.[25] To ease much pressure on crude oil, there is need to explore other sources of energy. Huge reserves of unexploited natural gas present such an opportunity because methane is cheaper than value-added petrochemicals like ethylene, benzene, and toluene. Using monometallic and bimetallic catalysts have been hampered by low methane conversion and limited product selectivity.[26] Even though natural gas production has steadily grown at an average of 2.2% for the last 10 years before 2016,[27] this energy production cannot meet population growth. Hence, there is need to explore more efficient technologies for conversion of methane into fuels and useful chemicals. The active components in the trimetallic catalysts were selected transition metals which are catalytically active in methane dehydroaromatization.[28] Previous studies have intimated that molybdenum is the most active metal in methane dehydroaromatization reaction when supported on HZSM-5 zeolite.[12] Tungsten has been found to enhance methane conversion and enhanced benzene yields.[29,30] When supported on HZSM-5, iron favors selectivity of aromatics and reduces coke selectivity.[31] HZSM-5 zeolite has a channel structure, inherent acidity, thermal stability,[32] and with high surface area.[33]

Therefore, the innovation of a trimetallic catalyst (Fe-W-Mo/HZSM-5) for application in methane dehydroaromatization will remediate against environmental pollution and provide a rubric for the development of a tunable commercial catalyst for use in methane

dehydroaromatization. In our previous work on trimetallic catalyst systems,[34] emphasis was placed on catalyst development and the effect of metal loading on methane conversion and product distribution. To the best of authors' knowledge, an in-depth analysis on the synergetic effect of each metal in Fe-W-Mo/HZSM-5 catalyst on methane conversion and product distribution has not been exhaustively reported, hence the main objective of this present study.

2 | EXPERIMENTAL

2.1 | Materials and methods

Materials used for preparation of the trimetallic catalyst were; ZSM-5 (NH_4ZSM-5), SiO_2:Al_2O_3 50%:50%, 99.9% pure from Zeolyst International, Iron nitrate Fe $(NO_3)_3.9H_2O$, 99.8% pure from Merk-USA, Ammonium heptamolybdate (AHM) $(NH_4)_6Mo_7O_{24}.4H_2O$, 99.9% pure from Merck-USA, Ammonium Para tungstate (APT) $(NH_4)_{10}W_{12}.4H_2O$, 99.8% from Merck-USA, methane-Argon feed mixture (1:1 mole) from Afrox-South Africa. Dried mixture of NH_4ZSM-5 was calcined at 550°C for 6 h to convert it into the hydrogen form (HZSM-5). Solutions of each catalyst precursor (Ferrite nitrate, APT, and AHM) in calculated quantities according to wt. % were prepared and stirred continuously for 2 h. A resultant solution of three catalyst precursors; Ferrite nitrate (FN), APT, and AHM in calculated quantities according to wt. % were dissolved in distilled water and stirred continuously for 2 h. The resultant solution was then deposited onto calculated amounts of HZM-5 drop-wise up to the point of incipient wetness. The mixture was left to dry overnight (12 h) at 110°C and then calcined at 550°C for 6 h to get a binary catalyst with corresponding metal oxides loaded on HZSM-5 (Fe_2O_3-WO_4-MoO_3/HZSM-5).

Prepared catalysts were synthesized by incipient wetness impregnation and characterized for phase identification and crystalline nature, shape, and size, and surface area.

2.2 | Catalyst characterization

Fabricated catalyst materials were characterized for phase identification using X-ray diffraction (XRD) technique. The instrument used in the analysis was BRUKER AXS (Germany). X-ray spectra of the catalysts were measured by a Rigaku PRINT 2500 V diffractometer operating in a coupled mode at Cu-K∝ radiation.

The specific surface area and distribution of pore sizes were measured at -196°C using Brunauer-Emmet Teller (BET) technique. The instrument used in the study was (Micromeritics Tristar II 3020). A Scanning electron microscope (FEI Nova Nano SEM 230) equipped with high-resolution immersion lens was used to analyse structural and textural properties of binary catalysts. The size and distribution of catalyst crystallites in each catalyst system was obtained using the Image-J software.

Thermogravimetric analysis of each catalyst was done using a differential thermogravimetric analyzer, TGA-6/DTG of Perkin Elmer (precision of temperature ±2°C) and microbalance sensitivity of <5μg, to monitor weight loss as functions temperature between 40 and 900°C. The experiments were carried out in air at atmospheric pressure, at a flow rate of 60 ml/min, at various linear heating rates of 5,10, 20, and 30 °C/minute. Small masses (10–25 mg) of each material were used to avoid mass and heat transfer limitations.

Information on morphology of carbon nanomaterial on the spent catalyst was obtained using an electron transmission instrument (JEOL JEM-1010-South Korea). Pretreatment of test samples involved ultrasonic dispersion of 3 mg of each catalyst material in isopropyl alcohol and sonicated for 10 min and dried for 15 min before loading the sample onto the TEM machine.

2.3 | Catalyst evaluation

Methane dehydroaromatization experimental runs were done in a custom-made stainless-steel reactor of dimensions (ID 8.6 mm, OD 12.6 mm and L-540 mm) as used in our other work[35] at atmospheric pressure. The experimental procedure entailed creating a catalyst bed holder (3 g of Quartz wool) in the middle part of the reactor. The reactor was pacified with nitrogen gas at (150 ml/min) and at 500°C for 15 min to expunge moisture and volatile organic matter from the reactor. The reactor was heated in an electrical furnace at 10°C/min to raise the reactor temperature from ambient temperature up to the set temperature. Methane-Argon gas mixture (1:1 mole) was introduced into the reactor at different temperatures, GHSV 960 $mlg^{-1}cat.h^{-1}$, and 1 atm. Reactor effluents were condensed before discharge into the conical flask to collect liquid hydrocarbons while the gaseous fractions were fed directly into an online gas chromatograph (Shimadzu 2014) equipped with TCD and FID detectors. Methane % conversion X as done elsewhere[36] and % selectivity S towards each hydrocarbon was calculated by applying Equations 1 and 2, respectively.

$$X = 1 - \frac{\text{number of moles of unreacted methane}}{\text{number of moles of methane fed into the reactor}} \times 100 \quad (1)$$

$$S = \frac{\text{number of moles of particular hydrocarbon produced}}{\text{Total number of moles of all the hydrocarbon products}} \times 100 \quad (2)$$

Equation (3) was used to calculate % coke selectivity.

$$\text{Coke Selectivity (\%)} = 100\% - \sum \text{Product selectivity \%} \quad (3)$$

3 | RESULTS AND DISCUSSION

Synthesized catalysts designated based on composition (wt. %) as shown in Table 1.

3.1 | Catalyst characterization

3.1.1 | XRD-analysis

As shown in Figure 1, the presence of HZSM-5 zeolite phase manifests itself at $2\theta = 8.0^{o}$,8.9^{o}, 14.9^{o}, 20.9^{o} and 23.2^{o} as classified in International Centre for Diffraction Data (ICDD File no. 00-044-002). In catalyst 2.7Fe2.7Mo/HZSM-5, peaks at $2\theta = 33.2^{o}$,35.7^{o},49.5^{o}, and 54.1^{o} confirm the presence of Fe_2O_3 phase as classified in (ICDD File no. 87-1166). Diffraction peaks at $2\theta = 34.3^{o}$, and 49.2^{o} are similar to those of MoO_3 as classified in (ICDD File no. 05-0508). Faint peaks at $2\theta = 23.2^{o}$,29.0^{o},42.1^{o}, and 50.4^{o} in catalyst 2.7 W2.7Mo/HZSM-5 confirm the presence of orthorhombic WO_3 as classified in (ICDD File no. 32-1394). Fe_2O_3 phase with peaks at $2\theta = 33.2^{o}$,35.7^{o},49.5^{o}, and 54.1^{o} and WO_3 with peaks at $2\theta = 23.2^{o}$,29.0^{o},42.1^{o}, and 50.4^{o} clearly manifest themselves in catalyst 2.7Fe2.7W/HZSM-5. When metal loading is equal in catalyst 1.8Fe1.8W1.8Mo/HZSM-5, Fe_2O_3, WO_3 and MoO_3 phases become very faint. This can be attributed to the fact that metal loading was very low and the catalyst crystallites were highly dispersed in the binary catalysts. After loading Fe_2O_3, WO_3 and MoO_3 onto HZSM-5, intensity of peaks became faint but did not shift. This implies that, loading Fe_2O_3, WO_3 and MoO_3 onto HZSM-5 did not distract the HZSM-5 structure.[37]

TABLE 1 Binary metal alloy catalyst systems.

Catalyst	Composition (wt. %)
2.7Fe2.7Mo/HZSM-5	2.7%Fe, 2.7%Mo and 94.6%HZSM-5
2.7 W2.7Mo/HZSM-5	2.7%W, 2.7%Mo and 94.6%HZSM-5
2.7Fe2.7 W/HZSM-5	2.7%Fe, 2.7%W and 94.6%HZSM-5
1.8Fe1.8W1.8Mo/HZSM-5	1.8%Fe, 1.8%W, 1.8%Mo and 94.6%HZSM-5

3.1.2 | SEM analysis

In Figure 2, tri-lobes and spherical nanoparticles are clearly seen in the SEM image of catalyst 2.7Fe2.7Mo/HZSM-5 with their sizes ranging from 2.6 to 23.0 nm. The mean particle size was 5.5 nm. A clear manifestation of these crystallites is an indication of little agglomeration during catalyst synthesis. Similar shapes of catalyst crystallites are clearly formed in catalyst 2.7W2.7Mo/HZSM-5 with their sizes ranging from 2.6 to 16.4 nm. In catalyst 2.7Fe2.7 W/HZSM-5, catalyst particle sizes ranged from 2.6 to 14.3 nm. When metal loading is equal in catalyst 1.8Fe1.8W1.8Mo/HZSM-5, definite tetrahedral and cubic nanoparticles are formed. Crystallite sizes ranged from 2.6 to 21.5 nm. Crystallite sizes in all the four catalyst materials ranged from 2.6 to 23.0 nm, implying that after calcination, all the catalyst crystallites were nanoparticles.

3.1.3 | B.E.T analysis

From BET results in Table 2, it can be seen that loading Fe, W, and Mo onto HZSM-5 greatly altered its initial

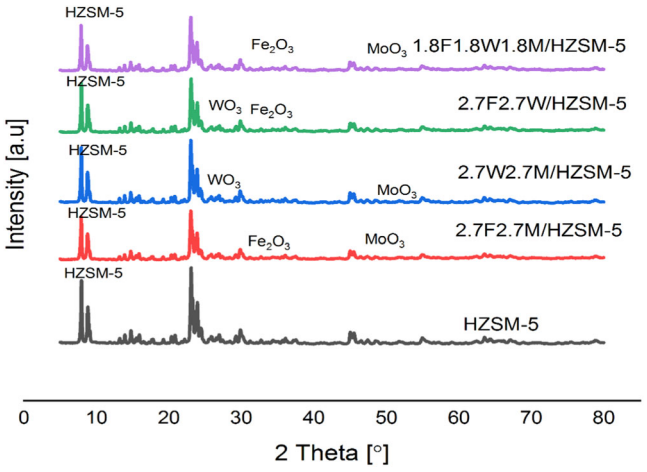

FIGURE 1 X-ray diffraction peaks for reference HZSM-5 zeolite and binary catalysts (2.7Fe2.7Mo/HZSM-5, 2.7W2.7Mo/HZSM-5, 2.7Fe2.7W/HZSM-5, and 1.8Fe1.8W1.8Mo/HZSM-5).

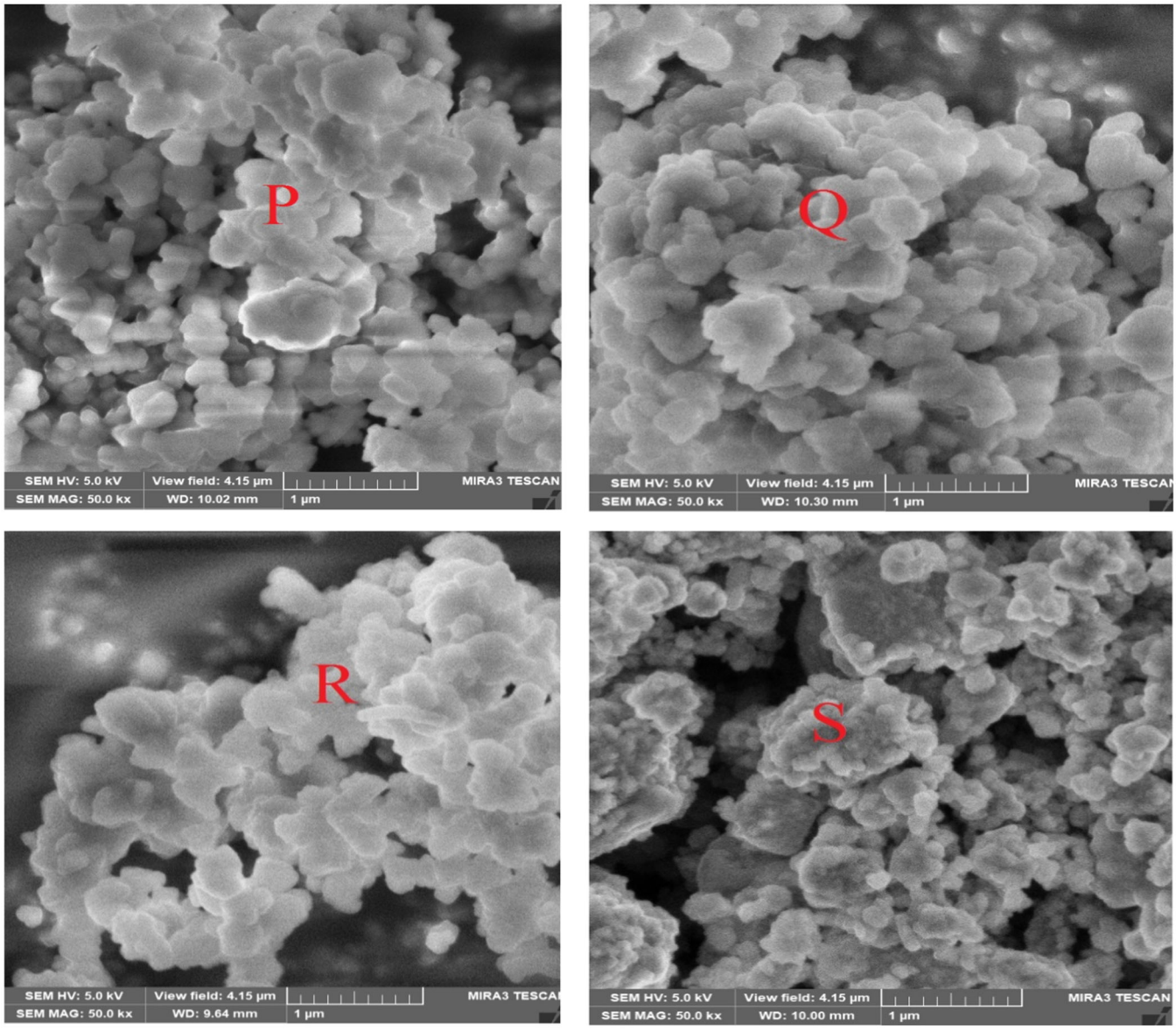

FIGURE 2 Scanning electron microscope images of catalyst P (2.7%Fe2.7%Mo/94.6%HZSM-5), Q (2.7%W2.7%Mo/94.6%HZSM-5), R (2.7%Fe2.7%W/94.6%HZSM-5) and S (1.8%Fe1.8%W1.8%Mo/94.6%HZSM-5).

surface and structural properties (surface area 496 m^2g^{-1}, pore volume 0.18 cm^3g^{-1} and pore size of 24.8 Å). Loading HZSM-5 with 5.4% iron, 5.4% tungsten, and 5.4% molybdenum, resulted in a reduction in zeolite surface area and pore volume and pore size. However, when two metals were loaded onto HZSM-5, a significant decrease in surface area and pore volume but instead, an increase in pore size was recorded in some catalyst systems.

Loading the zeolite with 2.7% iron and 2.7% molybdenum as it is typical in catalyst 2.7Fe2.7Mo/HZSM-5 decreased the surface area and pore volume of HZSM-5 zeolite by 41.5%, and 41.3% respectively. Despite this reduction, a change in catalyst pore size was insignificant. In catalyst 2.7 W2.7Mo/HZSM-5, surface area, and pore volume reduced but the pore size increased. A similar trend was observed in catalyst 2.7Fe2.7W/HZSM-5. Loading equal metal quantities on HZSM-5 support created a positive impact on the catalyst structural properties.

Based on the results obtained, the reference HZSM-5 support used in this present work is a mesoporous material with high surface area. Loading it with Fe_2O_3, WO_3 and MoO_3 reduced its surface area and pore volume. However, this scenario was true, only when metal loading is in excess of 2.0 wt. % because in a catalyst with equal metal loading (1.8Fe1.8W1.8Mo/HZSM-5), there was less reduction in zeolite surface area, insignificant reduction in pore volume, and a substantial

TABLE 2 Catalyst surface and structural properties.

Name of catalyst	Surface area (m^2/g)	Pore volume (cm^3/g)	Pore size (Å)
HZSM-5	495	0.17	24.7
5.4Fe/HZSM-5	340	0.13	24.0
5.4 W/HZSM-5	363	0.23	24.1
5.4Mo/HZSM-5	325	0.11	23.8
2.7Fe2.7Mo/HZSM-5	290	0.11	24.2
2.7 W2.7Mo/HZSM-5	242	0.13	34.2
2.7Fe2.7 W/HZSM-5	217	0.09	29.8
1.8Fe1.8W1.8Mo/HZSM-5	424	0.17	30.2

increase in pore size. Interestingly, when Fe was absent in catalyst 2.7W2.7Mo/HZSM-5, the catalyst pore size increased by 38% in reference to HZSM-5 support. It is therefore believed that, tungsten was responsible for pore size enhancement in the mesoporous HZSM-5 zeolite.

3.2 | Catalyst evaluation

3.2.1 | Effect of metal synergy

In Table 3, catalyst activity of HZSM-5, monometallic catalysts supported on HZSM-5, bimetallic catalysts supported on HZSM-5, and trimetallic catalysts were studied. Applying HZSM-5 catalyst methane conversion recorded 1% methane conversion but with 100% selectivity towards benzene. Monometallic Fe/HZSM-5 gave very good results in methane conversion and high coke yields. Monometallic W/HZSM-5 was little active in methane pyrolysis despite being highly selective towards benzene. A catalyst with Mo on/HZSM-5 support demonstrated high activity in methane conversion despite giving low C_2 hydrocarbon yields and low coke yields. Conversely, this catalyst most selective towards toluene.

Bimetallic 2.7W2.7Mo/HZSM-5 catalyst activated methane molecules more than any other catalyst despite yielding the highest amount of coke. Catalyst 2.7Fe2.7Mo/HZSM-5 did not show much activity in methane pyrolysis but demonstrated moderate selectivity towards benzene and coke. Catalyst 2.7Fe2.7W/HZSM-5 displayed outstanding results with 6.6% methane conversion, 53.4% selectivity towards benzene, and 22.5% coke selectivity. Interestingly, a catalyst system with all the three metal oxides (Fe_2O_3, WO_3 and MoO_3) on HZSM-5 recorded a reduction in methane conversion but with an improvement in selectivity towards C_2-hydrocarbons and coke. From these results, it was concluded that, iron and molybdenum on HZSM-5 are not very active in methane pyrolysis but show some substantial activity towards C_2 selectivity. Iron and molybdenum on HZSM-5 despite promoting methane conversion, they give rise to low benzene and high coke selectivity.

Each metal in a trimetallic catalyst system had a role to play i.e., Fe contributed to catalyst stability at this reaction conditions, selectivity towards C_2 hydrocarbons, and selectivity towards coke whereas W is desired for its activity in methane conversion. On the other hand, molybdenum is believed to have contributed immensely to evolution of (CH_3^+) before subsequent oligomerization into C_2H_6. The acidity and shape selectivity of HZSM-5 aided the conversion C_2 intermediates into benzene.

3.2.2 | Effect of activation time

In Figure 3, all the four catalysts exhibited a declining trend in methane conversion and selectivity towards hydrocarbons. After 1 h time on stream (TOS), catalyst activity values were high but gradually decreased due catalyst deactivation by coking. Deposition of coke reduces the kinetic diameter of benzene hence reducing its shape selectivity towards benzene formation.

Methane dehydroaromatization reaction starts with activation of C-H bond in a methane molecule by dehydrogenation. With regard to iron-based catalysts, carburized (Fe_3C) is the resultant active species formed after the induction period in methane activation.[38] Transformation of methane to carbon/C_2-hydrocarbons is facilitated by carbene which is a primary intermediate of activated methane molecules.[39] However, carbene is usually unstable on metallic sites and therefore its C-H bond bifurcates further to yield hydrogen. On the other hand, F_3C can stabilize carbene by formation of metal-carbene complex (C-Fe=CH_2) so that carbene can dimerize into ethylene, which is further transformed into aromatics in the zeolite acid sites. Therefore, a highly carburized catalyst is desired for high selectivity towards aromatics.

Methane conversion over monometallic Mo/HZSM-5 catalyst encompasses hydrogenation and dimerization of methane molecules on Mo species (MoO_3).[40] Upon interaction of this Mo species and the acid sites in the zeolite, an active component of the catalyst is formed.[41] Diffusion of MoO_3 species into the HZSM-5 zeolite channel occurs during catalyst calcination.

TABLE 3 Catalytic activity of each catalyst in methane dehydroaromatization at 750 °C, and GHSV 960 $mlg^{-1}cath^{-1}$, and 1 atm.

Sr/no.	Catalyst Name	CH_4 Conv. (%)	C_2 Selectivity (%)	C_2+ Hydrocarbon selectivity			Coke selectivity (%)
				Benzene (%)	Toluene (%)	Xylene (%)	
1.	HZSM-5	1.0	0.0	100	0.0	0.0	0.0
2.	Fe/HZSM-5	4.1	21.1	40.6	4.6	0.0	33.7
3.	W/HZSM-5	2.4	20.7	43.1	5.9	0.0	30.3
4.	Mo/HZSM-5	7.9	10.6	51.8	9.8	0.0	27.8
5.	2.7Fe2.7Mo/HZSM-5	3.9	12.3	45.6	11.6	0.0	30.6
6.	2.7 W2.7Mo/HZSM-5	15.2	8.5	44.2	10.1	0.0	37.2
7.	2.7Fe2.7W/HZSM-5	6.6	10.5	53.4	13.5	0.1	22.5
8.	1.8Fe1.8W1.8Mo/ HZSM-5	5.9	13.3	48.7	6.1	0.0	31.9

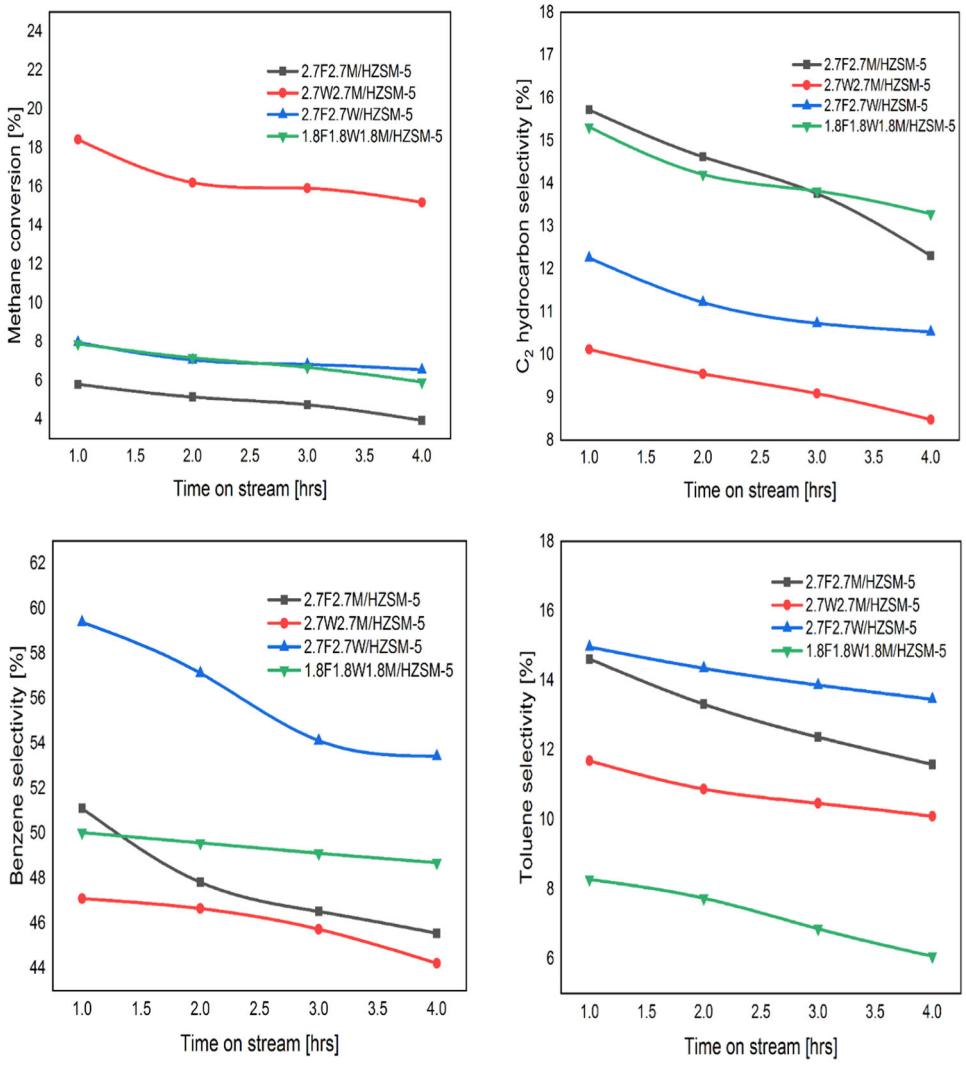

FIGURE 3 Catalyst activity in methane conversion and selectivity towards C_2 hydrocarbons, Benzene and Toluene in methane dehydroaromatization at different TOS, 750 °C, GHSV 960 $mlg^{-1}cath^{-1}$ and 1 atm.

Among group VI metals, tungsten has demonstrated the highest catalytic activity in dehydrogenation of methane into carbon and hydrogen directly[42]

In Figure 4, each catalyst activity depicts an upward trajectory when it comes to coke selectivity. Accumulation of coke on each catalyst increased with an increase in reaction time.

As shown in Figure 4, each catalyst exhibited a declining trend in xylene selectivity during each 4 h' time on stream. However, coke selectivity increased with an increase in reaction time.

3.3 | Characterization of spent catalyst

3.3.1 | TGA analysis of deposited carbon

Figure 5 shows TGA patterns of catalysts supported on HZSM-5. From the figure, there is no change in weight between 300°C and 400°C. Oxidation of deposited carbon nano material was complete at 600°C in a trimetallic catalyst with equal metal loading and catalyst 2.7Fe2.7Mo/HZSM-5. After the loss of residual moisture at 100°C, there was negligible change in weight. This is a characteristic of low temperature non- amorphous carbon material.

3.3.2 | Morphology of deposited carbon

In Figure 6, Transmission electron microscope images of carbon nanotubes (CTs) are clearly formed on catalyst 2.7Fe2.7Mo/HZSM-5. Micrographs of catalyst 2.7 W2.7Mo/HZSM-5 show images of irregularly shaped carbon nanomaterial. Therefore, Fe in the catalyst promoted the formation of carbon nanotubes on catalyst 2.7Fe2.7Mo/HZSM-5. The deposition pattern of these nanomaterial growth was similar to that reported by.[43] Few carbon nanotubes are seen on the spent 2.7Fe2.7 W/HZSM-5 catalyst. Even though Fe promoted the growth carbon nanotubes on catalyst 2.7Fe2.7Mo/HZSM-5, there was no formation of carbon nanotubes on catalyst 2.7Fe2.7W/HZSM-5. Therefore, tungsten promoted iron dispersion into the zeolite.

From literature, three types of coke (solid carbon deposits) can deposit on the spent catalyst based on temperature[44] as; graphitic coke at temperatures over 1153°C, amorphous carbon (carbon black) whose production increases with an increase in residence time and it is maximal between 600°C and 1153°C, and soot which is produced at shorter residence time (lower than 0.6 s) and at low temperatures (300–600°C). An increase in residence time or pressure enhances the formation of coke while the formation of solid carbon has been liked to methane formation.[45] The coking phenomenon occurs in various steps namely; dissociation of methane molecules to yield ethane, ethane to ethylene, ethylene to acetylene, and finally the transformation of acetylene into benzene. The growth of solid carbon (C_∞) occurs according to the following equation.

$$C_\infty + C_6H_6 = C_\infty + 3H_2 \quad (4)$$

Condensation of acetylene leads to benzene formation and finally to the growth of carbon nanoparticles. Evolved hydrogen from the pyrolysis reaction suppresses coke formation by saturating the radical active sites

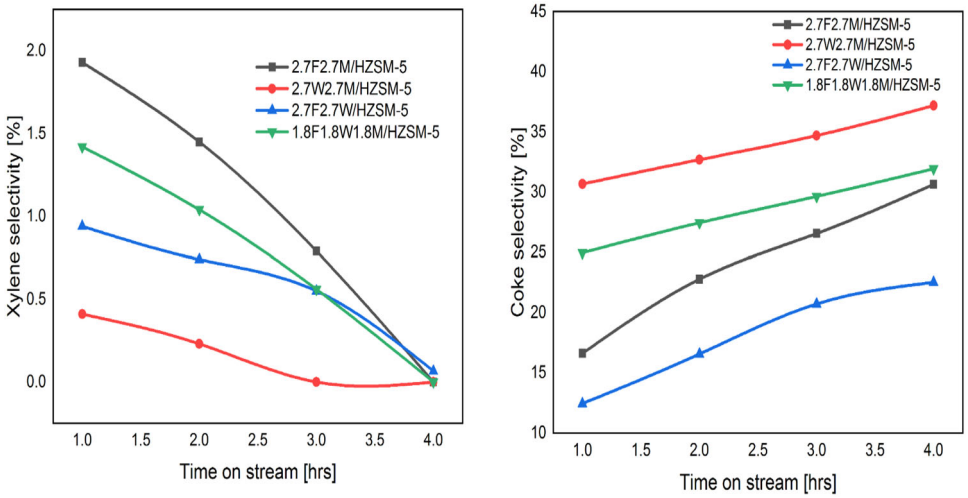

FIGURE 4 Catalyst selectivity towards Xylene and Coke in methane dehydroaromatization at different TOS, 750°C, GHSV 960 $mlg^{-1}cath^{-1}$ and 1 atm.

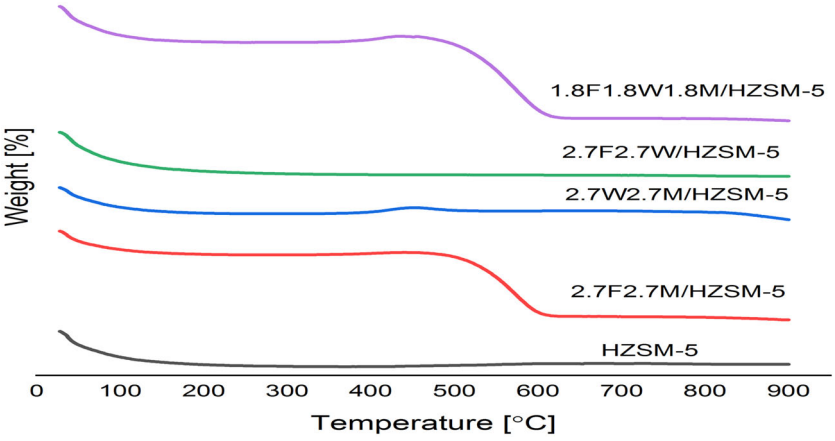

FIGURE 5 TGA pattern of catalysts; HZSM-5, 2.7Fe2.7Mo/HZSM-5, 2.7 W2.7Mo/HZSM-5, 2.7Fe2.7W/HZSM-5, and 1.8Fe1.8W1.8 M/HZSM-5.

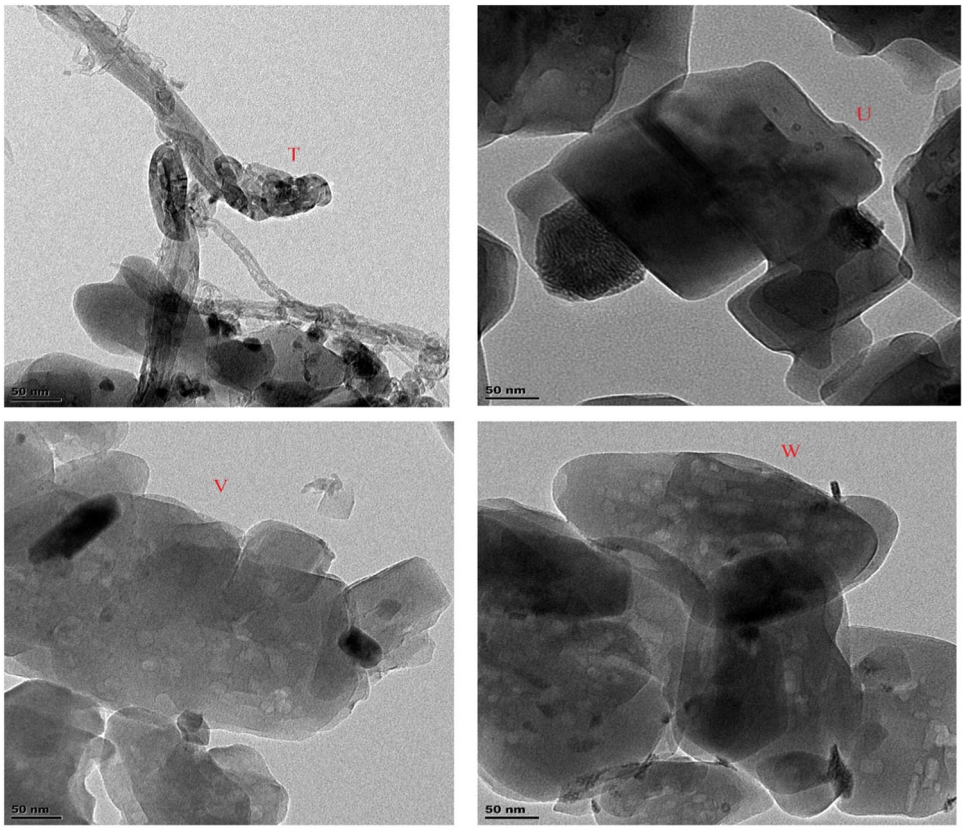

FIGURE 6 TEM images of catalyst T (2.7Fe2.7 Mo/HZSM-5), U (2.7 W2.7M/HZSM-5), V (2.7Fe2.7W/HZSM-5), and W (1.8Fe1.8W1.8Mo/HZSM-5).

hence, a decrease in the formation of acetylene and benzene.

Acetylene is a major source of coke while metal carbides act as intermediates. Common metallic catalysts used include nickel and iron. This type of coke is produced within the temperature range of 400–1053°C. The aromatic species (Ar-H) is the intermediate in the formation of coke as shown in Equation (5).

$$nAr-H \xrightarrow{-H_2} tars \xrightarrow[condensation]{nucleation} tar\ droplets \xrightarrow{-H_2} semi\ droplets \xrightarrow{-H_2} coke \quad (5)$$

This mechanism describes the growth of the coke layer involving acetylene with free radicals (methyl, ethyl, phenyl or benzyl) on the surface of deposited coke.

Low yields of carbon nanotubes on catalyst 2.7Fe2.7 W/HZSM-5 imply that catalyst crystallites were

highly dispersed in the HZSM-5 zeolite leading to ineffective activation of the C-H bond in methane. Our observation was concurrent with another observation reported in literature.[46] It is believed that Fe was responsible for complete dissociation of CH_4 into carbon nanotubes. Literature is replete with similar findings.[22] Even though Mo aided generation of CTs just like Fe, its presence in catalyst 1.8Fe1.8W1.8Mo/HZSM-5 was insignificant, thus rendering its inability to influence the generation of CTs due to high dispersion in the zeolite. A similar result was reported by another research group on nonoxidative methane activation.[37]

4 | CONCLUSIONS

This present study brings to the fore the synergistic effect of each metal in a trimetallic Fe-W-Mo/HZSM-5 catalyst system for application in methane dehydroaromatization. A catalyst system with only Fe and Mo on HZSM-5 support demonstrated little activity in methane pyrolysis despite being very selective towards C_2 hydrocarbons. A catalyst system with only tungsten and molybdenum on HZSM-5 support gave the best results in terms of methane conversion and selectivity towards coke. However, the same catalyst showed very little selectivity towards benzene. Such a catalyst, could be found useful in a process line where production of benzene is either not required or is to suppressed. Tungsten promoted good conversion and enhanced benzene selectivity. Iron promoted selectivity towards aromatics and suppressed coke formation. HZSM5 zeolite with its channel structure, inherent acidity, thermal stability, and high surface area played a crucial role in shape selectivity towards benzene.

A bimetallic catalyst with only 2.7% iron and 2.7% molybdenum on HZSM-5 showed little catalytic activity in methane conversion in comparison to catalyst 2.7W2.7Mo/HZSM-5 but was most selective towards benzene and coke. A 5.4% trimetallic catalyst with equal metal loading on HZSM-5 was highly selective towards C_2 hydrocarbons.

A study on methane dehydroaromatization can take different dimensions. Our present study focused on catalyst synthesis and catalyst activity in methane dehydroaromatization to demonstrate that, it is possible to synthesize and tune a metal-alloy catalyst depending on the products of interest in methane pyrolysis process line. In our view, synthesis and tuning of the tri-metallic Fe-W-Mo/HZSM-5 catalyst systems is feasible. Having established the synergistic effect of each metal in the trimetallic catalyst system, a rubric has been established for use to synthesize a commercial catalyst which can control the extent of methane conversion and product selectivity. However, further research work, which was not our main focus, can focus on studying the catalyst activity of Fe-W-Mo on different acidic supports and metal oxide composites and evaluate the catalyst performance. Further research can also focus on the mechanism of catalyst deactivation and regeneration of the spent catalyst so that it be used after several repeated heat cycles.

ACKNOWLEDGEMENTS

Our gratitude goes to Durban University of Technology, Technical University of Kenya, and University of Witwatersrand for their support.

ORCID

Yusuf. M. Isa http://orcid.org/0000-0001-8272-3402

REFERENCES

1. Brandt AR, Masnadi MS, Englander JG, Koomey J, Gordon D. Climate-wise choices in a world of oil abundance. *Environ Res Lett*. 2018;13(4):044027.
2. Faramawy S, Zaki T, Sakr AAE. Natural gas origin, composition, and processing: a review. *J Nat Gas Sci Eng*. 2016;34:34-54.
3. Gao Y, Zhang S, Sun H, Wang R, Tu X, Shao T. Highly efficient conversion of methane using microsecond and nanosecond pulsed spark discharges. *Appl Energy*. 2018;226:534-545.
4. De Klerk A. Sasol 2 and 3 facilities. *Fischer-Tropsch Refining*. Wiley-VCH: Weinheim; 2011:181-212.
5. Olah GA, Goeppert A, Prakash GS. *Beyond oil and gas: the methanol economy*. John Wiley & Sons; 2018.
6. Liu S, Wang L, Ohnishi R, Ichikawa M. Bifunctional catalysis of Mo/HZSM-5 in the dehydroaromatization of methane to benzene and naphthalene XAFS/TG/DTA/MASS/FTIR characterization and supporting effects. *J Catal*. 1999;181(2):175-188.
7. Wang L, Tao L, Xie M, Xu G, Huang J, Xu Y. Dehydrogenation and aromatization of methane under non-oxidizing conditions. *Catal Lett*. 1993;21(1-2):35-41.
8. Yuan S, Li J, Hao Z, et al. The effect of oxygen on the aromatization of methane over the Mo/HZSM-5 catalyst. *Catal Lett*. 1999;63(1-2):73-77.
9. Ma H, Ohnishi R, Ichikawa M. Highly stable performance of methane dehydroaromatization on Mo/HZSM-5 catalyst with a small amount of H 2 addition into methane feed. *Catal Lett*. 2003;89(1-2):143-146.
10. Fouty N, Carrasco J, Lima F. Modeling and design optimization of multifunctional membrane reactors for direct methane aromatization. *Membranes*. 2017;7(3):48.
11. Chen Y, Wang X, Luo X, Lin X, Zhang Y. Non-oxidative methane conversion using lead-and iron-modified albite catalysts in fixed-bed reactor. *Chin J Chem*. 2018;36(6):531-537.
12. Karakaya C, Kee RJ. Progress in the direct catalytic conversion of methane to fuels and chemicals. *Prog Energy Combust Sci*. 2016;55:60-97.
13. Xu Y, Liu S, Guo X, Wang L, Xie M. Methane activation without using oxidants over Mo/HZSM-5 zeolite catalysts. *Catal Lett*. 1995;30(1-4):135-149.
14. Solymosi F, Szöke A, Cserenyi J. Conversion of methane to benzene over mo 2 C and mo 2 C/ZSM-5 catalysts. *Catal Lett*. 1996;39(3-4):157-161.

15. Wang D, Lunsford JH, Rosynek MP. Characterization of a Mo/ZSM-5 catalyst for the conversion of methane to benzene. *J Catal*. 1997;169(1):347-358.
16. Wang D, Lunsford JH, Rosynek MP. Catalytic conversion of methane to benzene over Mo/ZSM-5. *Top Catal*. 1996;3(3-4):289-297.
17. Ohnishi R, Liu S, Dong Q, Wang L, Ichikawa M. Catalytic dehydrocondensation of methane with CO and CO2toward benzene and naphthalene on Mo/HZSM-5 and Fe/Co-modified Mo/HZSM-5. *J Catal*. 1999;182(1):92-103.
18. Ding W, Meitzner GD, Iglesia E. The effects of silanation of external acid sites on the structure and catalytic behavior of Mo/H–ZSM5. *J Catal*. 2002;206(1):14-22.
19. Burns S, Hargreaves JSJ, Pal P, Parida KM, Parija S. The effect of dopants on the activity of MoO3/ZSM-5 catalysts for the dehydroaromatisation of methane. *Catal Today*. 2006;114(4):383-387.
20. Rodrigues ACC, Monteiro JLF. The use of CH4/H2 cycles on dehydroaromatization of methane over MoMCM-22. *Catal Commun*. 2008;9(6):1060-1065.
21. Gaube J, Klein HF. Studies on the reaction mechanism of the Fischer–Tropsch synthesis on iron and cobalt. *J Mol Catal A: Chem*. 2008;283(1-2):60-68.
22. Xu Y, Wang J, Suzuki Y, Zhang ZG. Improving effect of Fe additive on the catalytic stability of Mo/HZSM-5 in the methane dehydroaromatization. *Catal Today*. 2012;185(1):41-46.
23. Xu Y, Wang J, Suzuki Y, Zhang ZG. Effect of transition metal additives on the catalytic stability of Mo/HZSM-5 in the methane dehydroaromatization under periodic CH4–H2 switch operation at 1073K. *Appl Catal A*. 2011;409-410:181-193.
24. Zeng JL, Xiong ZT, Zhang HB, Lin GD, Tsai KR. Nonoxidative dehydrogenation and aromatization of methane over W/HZSM-5-based catalysts. *Catal Lett*. 1998;53(1-2):119-124.
25. Sily PD, Noronha FB, Passos FB. Methane direct conversion on Mo/ZSM-5 catalysts modified by pd and ru. *J Nat Gas Chem*. 2006;15(2):82-86.
26. Bajec D, et al. Nonoxidative methane activation, coupling, and conversion to ethane, ethylene, and hydrogen over Fe/HZSM-5, Mo/HZSM-5, and Fe–Mo/HZSM-5 catalysts in packed bed reactor. *Int J Energy Res*.2019;43(13):6852-6868.
27. Bajec D, et al. Micro-kinetics of non-oxidative methane coupling to ethylene over Pt/CeO2 catalyst. *Chem Eng J*. 2020;396:125182.
28. Shu Y, Ichikawa M. Catalytic dehydrocondensation of methane towards benzene and naphthalene on transition metal supported zeolite catalysts: templating role of zeolite micropores and characterization of active metallic sites. *Catal Today*. 2001;71(1):55-67.
29. Weckhuysen BM, Wang D, Rosynek MP, Lunsford JH. Conversion of methane to benzene over transition metal ion ZSM-5 zeolites. *J Catal*. 1998;175(2):338-346.
30. Fila V, Bernauer M, Bernauer B, Sobalik Z. Effect of addition of a second metal in Mo/ZSM-5 catalyst for methane aromatization reaction under elevated pressures. *Catal Today*. 2015;256:269-275.
31. Aboul-Gheit AK, Awadallah AE, El-Kossy SM, Mahmoud ALH. Effect of pd or ir on the catalytic performance of Mo/H-ZSM-5 during the non-oxidative conversion of natural gas to petrochemicals. *J Nat Gas Chem*. 2008;17(4):337-343.
32. Ali MA, Tatsumi T, Masuda T. Development of heavy oil hydrocracking catalysts using amorphous silica-alumina and zeolites as catalyst supports. *Appl Catal, A*. 2002;233(1):77-90.
33. Fujikawa T, Idei K, Ebihara T, Mizuguchi H, Usui K. Aromatic hydrogenation of distillates over SiO2-Al2O3-supported noble metal catalysts. *Appl Catal A*. 2000;192(2):253-261.
34. Musamali RW, Isa YM. Non-oxidative conversion of methane into various petrochemical grades over tunable tri-metallic Fe-W-Mo/HZSM-5 catalyst systems. *J Saudi Chem Soc*. 2023;27:101657.
35. Aliyu UM, Rathilal S, Mustapha SI, Musamali R, Tetteh EK. Hydrothermal synthesis of kaolin-based ZSM-5 zeolite: effect of synthesis parameters and its application for bioethanol conversion. *Catal Commun*. 2023;182:106750.
36. Musamali R, Isa YM. A novel catalyst system for methane decomposition. *Int J Energy Res*. 2018;42(14):4372-4382.
37. Bajec D, Kostyniuk A, Pohar A, Likozar B. Nonoxidative methane activation, coupling, and conversion to ethane, ethylene, and hydrogen over Fe/HZSM-5, Mo/HZSM-5, and Fe–Mo/HZSM-5 catalysts in packed bed reactor. *Int J Energy Res*. 2019;43(13):er.4697.
38. Denardin F, Perez-Lopez OW. Tuning the acidity and reducibility of Fe/ZSM-5 catalysts for methane dehydroaromatization. *Fuel*. 2019;236:1293-1300.
39. Tan P. Active phase, catalytic activity, and induction period of Fe/Zeolite material in nonoxidative aromatization of methane. *J Catal*. 2016;338:21-29.
40. Solymosi F, Bugyi L, Oszkó A, Horváth I. Generation and reactions of CH2 and C2H5 species on Mo2C/Mo (111) surface. *J Catal*. 1999;185(1):160-169.
41. Zhang C-L, Li S, Yuan Y, Zhang WX, Wu TH, Lin LW. Aromatization of methane in the absence of oxygen over mo-based catalysts supported on different types of zeolites. *Catal Lett*. 1998;56(4):207-213.
42. Aboul-Gheit AK, Awadallah AE. Effect of combining the metals of group VI supported on H-ZSM-5 zeolite as catalysts for non-oxidative conversion of natural gas to petrochemicals. *J Nat Gas Chem*. 2009;18(1):71-77.
43. Chen P, Zhang HB, Lin GD, Hong Q, Tsai KR. Growth of carbon nanotubes by catalytic decomposition of CH4 or CO on a Ni-MgO catalyst. *Carbon*. 1997;35(10):1495-1501.
44. Guéret C, Billaud F, Fixari B, Le Perchec P. Thermal coupling of methane, experimental investigations on coke deposits. *Carbon*. 1995;33(2):159-170.
45. Fau G, Gascoin N, Steelant J. Hydrocarbon pyrolysis with a methane focus: A review on the catalytic effect and the coke production. *J Anal Appl Pyrolysis*. 2014;108:1-11.
46. Li J, Dong L, Xiong L, et al. High-loaded NiCuSiO2 catalysts for methane decomposition to prepare hydrogen and carbon filaments. *Int J Hydrogen Energy*. 2016;41(28):12038-12048.

How to cite this article: Musamali RW, and Isa YM. Synergetic effect of iron and tungsten on molybdenum-doped HZSM-5 zeolite in catalytic methane dehydroaromatization. *Energy Sci Eng*. 2024;12:5008-5018. doi:10.1002/ese3.1919